Journal of Engineering Mathematics **31:** 205–234, 1997.

Upward buoyant filtration combustion

A. P. ALDUSHIN[1], B. J. MATKOWSKY[2] and D. A. SCHULT[2]
[1]*Institute of Structural Macrokinetics Russian Academy of Sciences 142432 Chernogolovka, Russia*
[2]*Department of Engineering Sciences and Applied Mathematics Northwestern University, Evanston, IL 60208, U.S.A.*

Received 21 March 1996; accepted in revised form 31 October 1996

Abstract. Heterogeneous combustion in a porous sample with only the top and bottom ends of the sample open to gas flow is considered. Gas enters the sample due to buoyant upward convection. That is, ignition at the bottom produces an upwardly propagating filtration combustion wave which induces hot gas to rise, thus pulling cool, fresh gas containing oxidizer in through the bottom of the sample. The gas moves through the solid products to reach the reaction zone just as in forced forward filtration combustion. In contrast to forced forward filtration combustion, in which the incoming gas flux is fixed by an external source, here the incoming gas flux is determined by the combustion process itself. That is, the incoming gas flux is determined by the burning temperature which in turn is affected by the incoming gas flux. Thus, a feedback mechanism exists which hinders ignition of the samples, but also makes the wave hard to extinguish, once it has formed. A one-dimensional model is analyzed and two types of wave structure, termed reaction-leading and reaction-trailing according as the reaction occurs at the leading or trailing edge of the heated region of the sample, respectively, are determined. For each structure, two solution modes are described, termed stoichiometric and kinetically controlled, according as the rate of oxygen supply or the kinetics controls propagation of the wave. In each of these four situations, expressions are derived for the evolution of the burning temperature, propagation velocity, incoming gas flux, degree of oxidizer consumption and degree of fuel conversion as the wave moves through the sample. In addition, profiles for the temperature are described. Analysis of the case where significant heat is lost through the sides of the sample leads to extinction limits and demonstrates the sensitivity of the wave structure to changes in external heat losses.

Key words: porous medium, combustion, gravity, buoyancy, traveling waves

1. Introduction

Filtration combustion (FC) describes applications such as smoldering, underground burning of coal and petroleum beds, where combustion has been known to continue for many months, and self-propagating high temperature synthesis (SHS) of advanced materials, which is a promising synthesis technique that uses the internal energy of the combustion reactions, rather than an external energy source, such as a furnace to produce desired products. In its most general form, FC describes a heterogeneous solid/gas reaction within a porous matrix where fluid flow through the matrix is an important aspect of the combustion process. In this paper, we consider a model of upward buoyant FC.

Filtration of gas through a burning porous matrix can be caused by a number of mechanisms. Filtration caused by external forcing of gas into one end of a sample is reffered to as forced filtration [1–8]. Filtration induced by the combustion process itself, *e.g.* when gas is consumed in the reaction [1, 9, 10], is referred to as natural filtration. Filtration can also be caused by forces such as gravity. Buoyant FC refers to combustion in a porous medium where filtration occurs due to gravity-induced buoyancy forces. We discuss buoyant FC in which the sample is ignited from below, leading to a combustion wave which propagates upward toward the top of the sample (see Figure 1). The sides of the sample are impermeable to gas (no cross-flow) so that hot gas rises and exits the top, inducing cool gas to enter through the bottom to replace the hot gas. When the gas moves in the same direction as the combustion wave, it is called

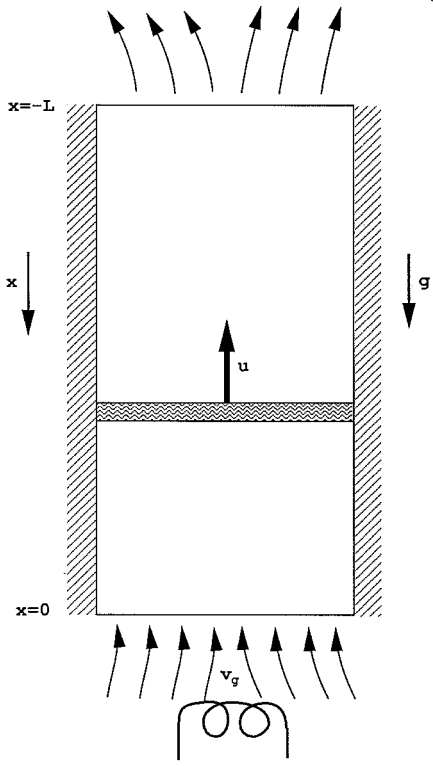

Figure 1. A sketch of the configuration for Upward Buoyant Filtration Combustion.

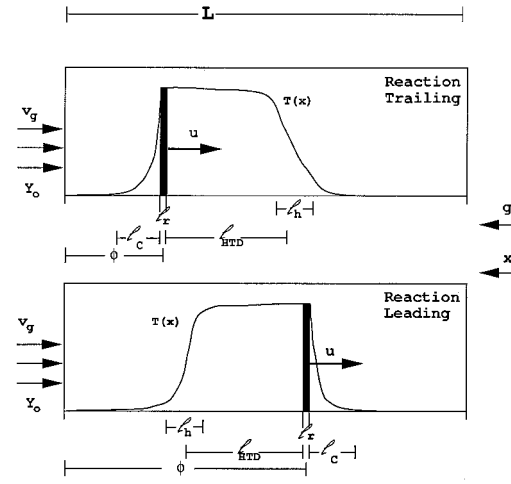

Figure 2. A sketch of the temperature profiles for reaction-leading and reaction-trailing solution structures, indicating the length scales for the reaction zone, l_r, combustion layer l_C, heat-transfer layer l_h, localized high-temperature domain l_{HTD} and sample size L.

co-flow or forward-flow combustion. In contrast, when the gas and the combustion wave move in opposite directions, it is called counter-flow or opposed-flow combustion. When gas enters through the sides of the sample, it is referred to as cross-flow combustion. In this paper, we consider upward forward buoyant FC.

Upward smoldering combustion experiments [11, 12] have demonstrated unsteady propagation in that the wave speeds up as it propagates. In these studies, oxygen is completely consumed in the reaction, the burning temperature is approximately constant and ignition time increases with the length of the sample. Solutions of our model describe the quasi-steady behavior of the observed combustion waves away from the top and bottom of the sample where end effects dominate.

Most applications of FC involve complex chemical reaction schemes. We may often simplify these schemes by considering the limiting steps in the process. For example, in smoldering of organic materials, the process can be simplified to consideration of three reactions [4], 1) oxidative decomposition of the virgin fuel into char and product gases, 2) endothermic pyrolysis which also converts the virgin fuel to a type of char but in an endothermic process that does not require oxygen, 3) highly exothermic oxidation of the char. For opposed-flow configurations, where oxygen passes through the fresh fuel, oxidative decomposition dominates endothermic pyrolysis as the major producer of char. In most situations, oxygen is

depleted in this process, so that oxidation of the char does not occur and it can be modeled as a one-step reaction. For forward-flow configurations, oxygen enters through the product region and is not plentiful ahead of the reaction in the region containing fresh fuel. Thus, endothermic pyrolysis dominates oxidative decomposition in the formation of char. The heat required for the endothermic process is provided by the oxidation of the resulting char. The energy released during oxidation is much greater than that consumed in pyrolysis. Thus, the process may be approximated by a one-step reaction which neglects the pyrolysis stage and considers only the oxidation stage [13].

Each application of FC is associated with a specific reaction scheme, so that any general theory of FC can only describe qualitative features of the process which are independent of the details of the reaction scheme.

We describe the qualitative features of upward buoyant FC using the simple, yet general, one-step reaction scheme,

$$\text{Solid Reactant} + (\mu)\ \text{Gaseous Reactant} \rightarrow (1-\mu_g)\ \text{Solid Product} + (\mu_g+\mu)\ \text{Gaseous Product}. \tag{1.1}$$

We account for the possibility that one of the two products does not exist by the stoichiometric parameter μ_g which measures the net mass of gas produced (that produced minus that consumed) in the reaction of one unit mass of solid reactant. If no solid product exists $\mu_g = 1$. If no gaseous product exists, $\mu_g = -\mu$ where μ measures the mass of gaseous reactant consumed in the reaction of one unit mass of solid reactant.

Upward buoyant forward FC is similar to forced forward FC in that the oxidizer (gas reactant) passes through the product region before reacting with the fuel (solid reactant). It differs from forced filtration, in which the gas flux is fixed by an external source, in that here gravity causes the gas to enter the sample and the resulting buoyant flux is determined by the combustion wave itself. Despite the differences, comparison of the upward buoyant and forced forward cases is useful.

We employ a one-temperature model, which is appropriate for the case of a high rate of heat transfer between the solid and the gas. Analysis of forced forward FC models [3, 5, 14] shows that the solutions exhibit a localized high-temperature domain (HTD) in which the temperature is essentially constant, with transition layers, ahead of and behind the HTD, in which the temperature decreases rapidly to the ambient temperature. One transition layer, termed the combustion layer, consists of a region in which thermal diffusion dominates and a second narrow region within the combustion layer termed the reaction zone, in which reaction as well as diffusion are significant. The other layer is due to the heat exchange between solid and gas and is termed the heat-transfer layer. The propagation velocities of the two layers are, in general, different. The velocity of the heat-transfer layer is determined by the heat exchange between the solid and gaseous phases, while the velocity of the combustion layer is determined by the oxidizer supply and the kinetic rate of the reaction. Two solution structures are determined by the relative velocities (and thus, after transients, the relative positions) of the two layers. For relatively high ambient oxidizer concentrations, the combustion layer preceeds the heat-transfer layer and the structure is called reaction-leading. For lower oxidizer concentrations, a reaction-trailing structure arises in which the heat-transfer layer lies ahead of the combustion layer. We will show that the same structures arise in upward buoyant FC (see Figure 2).

The solutions of forced forward models are not steady-state solutions, since the layers move at different velocities and, thus, the HTD expands as the wave propagates through the sample. For samples much larger than the width of the combustion layer, this expansion does not affect the propagation velocity and burning temperature, because they are determined on the scale of the combustion layer, where time variation is negligible.

For upward buoyant combustion, there is another source of variation. As the HTD expands, more of the gas contained in the sample is heated, increasing buoyancy, thus increasing the incoming gas flux. The expansion rate of the HTD increases with the gas flux, so that a positive feedback exists which causes the solution to vary at an ever increasing rate. On the scale of the combustion layer, the time variation is still small, as long as the sample is much longer than the combustion layer.

For each of the reaction-leading and reaction-trailing structures in the forced forward case, there are two solution types. Stoichiometric combustion occurs when the incoming mass flux is relatively small, so that all the oxidizer is consumed in the reaction. Note that all the fuel is consumed as well, since the oxidizer reacts with the fuel it first encounters, so that the reaction converts all the fuel before it proceeds along the sample. In stoichiometric combustion, the propagation velocity of the combustion layer is determined by the incoming gas mass flux. The second solution type is referred to as kinetically controlled. For relatively large incoming mass flux, the combustion layer moves faster than the velocity corresponding to stoichiometric conditions, and one reactant is in excess. The wave velocity is determined by the kinetics of the reaction. For the reaction-leading (trailing) structure, the kinetically controlled solution allows excess oxidizer (fuel) to pass through the combustion layer into the cool region ahead of (behind) the wave. For upward buoyant combustion, the incoming gas flux increases as the wave propagates along the sample. Thus, the solution type is determined by the level of buoyancy, and may change from stoichiometric to kinetically controlled as the combustion wave propagates.

Super-adiabatic temperatures, in which the burning temperature exceeds the temperature obtained from burning the same reactants in a spatially homogeneous fashion without heat losses, arise in forced forward FC. This is due to the fuel being preheated by the gas which absorbs heat from the burned solid as it passes through the product region and transports it to the fresh solid fuel. The level of the temperature in the HTD is determined by an energy balance between the heat released in the reaction and the heat needed to raise the temperature of the material added to the HTD as it expands. If the velocities of the layers are very close, the amount of material added to the HTD due to expansion is small and the resulting temperature is large, since the HTD is essentially constant and the heat release in the reaction leads to an increased temperature. The temperature is theoretically unbounded as the velocities of the two layers approach one another. In reality, effects not included in the model, such as the decomposition of the products, keep the temperatures finite. Super-adiabatic temperatures due to forward flow have been found experimentally long ago [15, 16]. Super-adiabatic temperatures are also achieved in upward buoyant FC.

We also consider the effect of heat losses to the external environment. Heat losses may restrict the size of the HTD and thus the incoming gas flux. In this case, the temperature may decrease to the ambient value in a larger region, rather than in a thin layer, and the entire structure may then move with a single velocity rather than the leading and trailing layers moving with separate velocities. In general, this single velocity varies with the fraction of the sample that has burned, which changes slowly in time for long samples as the wave propagates. Conditions exist however, where it does not vary at all and we have a traveling

wave solution. A traveling wave solution can be found for the non-adiabatic model under the condition that the gas flux is not changed during the combustion process, *e.g.* if there is negligible net production of gas and little change in the permeability of the sample.

Heat losses become important when the HTD becomes sufficiently long that temperature decreases, due to external heat losses, in large portions of the sample, rather than solely in the heat-transfer layer. In this case, the wave no longer exhibits a heat-transfer layer and the HTD is restricted from growing longer. The entire wave moves with the single velocity of the combustion layer. In general, the effect of heat losses is most easily seen in long samples after sufficiently long times. We model the effect of heat loss by a term in the energy equation which is proportional to the difference between the temperature in the sample and the ambient temperature. This constant of proportionality depends on the cross section of the sample and the insulation at the walls as well as other factors. The non-adiabatic case differs from the adiabatic case in that the HTD is determined by cooling to the external environment and does not necessarily expand as the wave moves through the sample. As a result, traveling-wave solutions are possible in the long-time limit.

When heat loss is significant, the HTD is shorter than for the adiabatic case and it may not expand with time. The amount of hot gas in the sample is lower and buoyancy forces must be sufficiently strong to drive gas flux without large heated regions. This occurs for large initial gas densities, large gravitational acceleration, or high permeability (low friction coefficient) of the porous material. Combustion may occur under these strong buoyancy conditions, even though heat losses are significant.

We find that the buoyancy causes the wave to become more intense as it moves through the sample. Burning temperature, propagation velocity and induced gas flux all increase with the burned portion of the sample. In addition, buoyancy can cause the waves to change from the stoichiometric mode to the kinetically controlled mode at a critical position along the sample. The transition point corresponds to a critical fraction of the sample which is burned. This critical fraction depends on buoyancy.

We describe boundaries in parameter space between regions that support reaction-leading and trailing waves as well as stoichiometric mode *vs*. kinetically controlled mode.

Heat losses may lead to extinction only in the kinetic mode. Stoichiometric waves become kinetically controlled with increased heat losses before they are extinguished.

To describe upward buoyant FC, we make the following assumptions: 1) that the configuration can support essentially one-dimensional solutions, 2) that the activation energy is large, so that the reaction zone is thin compared to the combustion layer, 3) that the heat exchange between gas and solid is sufficiently fast compared to the reaction process that a one temperature model is valid, 4) that the ambient pressure is much larger than the hydrostatic-pressure drop across the sample, so that pressure is approximately constant in the sample, 5) that the initial density of gas is much less than that of solid so that velocity of the gas is large compared to the propagation velocity when any appreciable conversion occurs, and so that the effective Lewis number of the porous medium is large, 6) that the permeability of the sample is sufficiently large that gravitational forces can induce gas flow, and 7) that the reaction dependence on the reactant concentrations is weak relative to the temperature dependence and can be approximated by a step function. These assumptions allow us to derive an analytical solution of the problem, for which we can determine the fundamental characteristics of buoyancy-driven FC waves, such as combustion velocity, combustion temperature, product composition, widths of the HTD and transition layers, and the structure of the wave corresponding to different modes of propagation.

In Section 1.1 we introduce the mathematical model and describe the physical assumptions necessary to simplify the model for tractability. In Section 2 we describe solutions for the adiabatic case. In Section 3 we consider the effect of heat losses to the external environment. Finally, Section 4 is devoted to discussion and conclusions.

1.1. MATHEMATICAL MODEL

The model of buoyant combustion consists of equations describing conservation of energy, gas mass, oxidizer mass, solid-reactant mass, and gas momentum, as well as an equation of state, and appropriate boundary and initial conditions. We consider a one-dimensional model in which gas can pass through the top and bottom of the sample. The sides are considered to be gas impermeable, though heat losses to the external environment can occur through the sides. Such heat losses are modeled as a global heat-loss mechanism by a term in the energy equation which is proportional to the difference in temperature between the sample and the external environment. The constant of proportionality, $\tilde{\alpha}$, is related to the cross-sectional area of the sample and the type of insulation at the side walls. A one-temperature model is used and is valid for combustion waves where the time of heat transfer between solid and gas phases in the sample is so short that the heat transfer can be considered to be instantaneous, which is the case for typical FC processes. The following equations describe upward filtration combustion in a sample of length L, in the laboratory coordinate system. The model is written in terms of the temperature $\tilde{T}$, degree of conversion $\eta = 1 - (\tilde{\rho}_s/\tilde{\rho}_{so})$, where $\tilde{\rho}_s$ is the effective density of the solid with $\tilde{\rho}_{so}$ its initial value, effective gas pressure $\tilde{P} = \pi \tilde{P}_{\text{actual}}$ where π is the porosity of the sample, density $\tilde{\rho}_g$, and the velocity $\tilde{v}_g$, as well as oxidizer mass fraction $\tilde{Y}$.

$$\tilde{c}_1 \frac{\partial \tilde{T}}{\partial \tilde{t}} - c_g \tilde{\rho}_g \tilde{v}_g \frac{\partial \tilde{T}}{\partial \tilde{x}} = \lambda \frac{\partial^2 \tilde{T}}{\partial \tilde{x}^2} + \tilde{Q} \tilde{\rho}_{so} \tilde{W} - \tilde{\alpha}(\tilde{T} - \tilde{T}_0), \tag{1.2}$$

$$\frac{\partial \tilde{\rho}_g}{\partial \tilde{t}} - \frac{\partial \tilde{\rho}_g \tilde{v}_g}{\partial \tilde{x}} = \mu_g \tilde{\rho}_{so} \tilde{W}, \tag{1.3}$$

$$\frac{\partial \tilde{\rho}_g \tilde{Y}}{\partial \tilde{t}} - \frac{\partial \tilde{\rho}_g \tilde{v}_g \tilde{Y}}{\partial \tilde{x}} = \frac{\partial}{\partial \tilde{x}} D \tilde{\rho}_g \frac{\partial \tilde{Y}}{\partial \tilde{x}} - \mu \tilde{\rho}_{so} \tilde{W}, \tag{1.4}$$

$$\frac{\partial \eta}{\partial \tilde{t}} = \tilde{W}, \qquad \frac{\partial \tilde{P}}{\partial \tilde{x}} - \tilde{f} \tilde{v}_g - \tilde{\rho}_g g = 0, \tag{1.5–1.6}$$

$$\tilde{P} = \tilde{R} \tilde{\rho}_g \tilde{T}, \qquad \tilde{c}_1 = \tilde{\rho}_{so} c_s (1 - \mu_g \eta c_g / c_s) + \tilde{\rho}_g c_g. \tag{1.7–1.8}$$

Boundary conditions corresponding to upward propagation are

$$\text{at } \tilde{x} = -L\text{:} \quad \tilde{P} = \tilde{P}_o - g \tilde{\rho}_{go} L, \quad \frac{\partial \tilde{T}}{\partial \tilde{x}} = 0, \quad \frac{\partial \tilde{Y}}{\partial \tilde{x}} = 0, \quad \eta = 0, \tag{1.9}$$

$$\text{at } \tilde{x} = 0\text{:} \quad \tilde{P} = \tilde{P}_o, \quad \tilde{T} = \tilde{T}_o, \quad \tilde{Y} = \tilde{Y}_o. \tag{1.10}$$

Initial conditions are discussed below.

Parameters of the system include the heat capacities c_g and c_s for the gas and solid, respectively, the effective densities $\tilde{\rho}_g$, $\tilde{\rho}_s$, $\tilde{\rho}_{go}$ and $\tilde{\rho}_{so}$ which take into account the porosity π

of the sample (thus, $\tilde{\rho}_g = \pi\tilde{\rho}_{g\,\text{actual}}$ and $\tilde{\rho}_s = (1-\pi)\tilde{\rho}_{\text{actual}}$), the thermal conductivity of the mixture λ, the permeability of the samples as measured by the filtration coefficient $\tilde{f}$ which is taken to be a known constant $\tilde{f}_-$ for the fuel region, and a possibly different constant $\tilde{f}_+$ for the product region, the diffusivity D of the oxidizer through the gas, the universal gas constant divided by the molecular weight of the gas $\tilde{R}$, the gravitational acceleration g, the length of the sample L, and the heat released in the reaction $\tilde{Q}$, the stoichiometric ratio of the mass of oxidizer and solid fuel consumed in the reaction μ and a similar ratio for the net mass of gas μ_g released in the reaction to mass of solid fuel consumed. Note that $\mu_g < 0$ if more gas is consumed than released in the reaction. The temporal and spatial variables are denoted $\tilde{t}$ and $\tilde{x}$, respectively, and the reaction rate $\tilde{W}$ depends on the temperature, and the concentration of each reactant

$$\tilde{W} = H(1-\eta)H(\tilde{Y})K_0\,\mathrm{e}^{-\frac{\tilde{E}}{\tilde{R}\tilde{T}}}. \tag{1.11}$$

Here H is the Heaviside step function, so that the kinetic dependence on the reactants is referred to as zero-order reaction dependence, which is a good approximation for reactions with a weak dependence on reactant concentrations. The temperature dependence is taken to be of Arrhenius type with activation energy $\tilde{E}$, pre-exponential factor K_0, and gas constant R.

We assume that the length L of the sample is much larger than all other length scales except that of pressure changes due to hydrostatic pressure. In particular, the sample is much longer than the length of the combustion layer $l_c (L \gg l_c)$. We assume that the pressure drop across the sample due to buoyant hydrostatic forces is much less than the ambient pressure, so that the pressure is essentially constant throughout the sample. This is reasonable for all but extremely high-gravitational environments. We consider gas velocities to be much larger than the velocity of propagation $\tilde{u}$ of the combustion wave ($\tilde{v}_g \gg \tilde{u}$), which is the case when the permeability of the porous matrix is sufficiently high to allow gas fluxes to be comparable to the mass-conversion rate of the solid ($\tilde{\rho}_{so}\tilde{u}$). Finally, we use large activation energy asymptotics to consider the resulting narrow reaction region as a front.

We seek propagating-wave solutions, and therefore transform to a moving-coordinate system attached to the site ($\tilde{x} = -\phi$) where the reaction rate is maximal. In the limit of large activation energy the region where the reaction is significant shrinks to a front and the coordinate is attached to the front. We denote the new spatial coordinate by $\hat{x} = \tilde{x} + \phi(\tilde{t})$ and the velocity of the front as $\tilde{u} = \phi_{\tilde{t}}$. In general, steady-state traveling-wave solutions do not exist for this system. As with other combustion systems in which the flux is determined by processes inside the sample, the wave changes its characteristics as it moves along the sample. In particular, the solution depends on the relative position $\varphi = \phi/L$ of the front, since buoyant forces increase as more of the sample is heated.

Figure 2 shows a sketch of the temperature profile in the sample for the reaction-leading and reaction-trailing structures. The characteristic length scales for the reaction zone l_r, combustion layer l_C, HTD l_{HTD}, heat-transfer layer l_h, and sample size L are indicated. The length scale of cooling l_α, which is not shown, is the scale on which the temperature profile decays due to external heat losses. Thus, l_α increases as heat losses decrease. In our analysis the reaction zone is assumed to be thin $l_r \ll l_c$, so that the narrow reaction zone, or front approximation, is valid, and the sample is assumed to be long, $L \gg l_c, l_h, l_\alpha$. We consider separately the cases when heat losses are negligible ($l_{\text{HTD}} \ll l_\alpha$) and when they are not.

In the next section, we simplify the model using the above assumptions by considering the momentum equation (Darcy's Law) (1.6) to derive a leading-order integral relation between

the gas flux induced by buoyancy forces and an appropriate average temperature in the sample. Then we use this relation in place of the momentum equation in our model. We also determine a relation between the position of the heat-transfer layer and that of the combustion layer, and we replace the spatially distributed reaction terms with jump conditions across the reaction site $\hat{x} = 0$. In subsequent sections, we describe solutions to this system.

1.2. SCALING AND THIN REACTION ZONES

In this section, we use the relative scales of the problem to reduce the momentum equation to a more tractable form, to determine the position of the heat transfer layer relative to the combustion layer, and to replace the spatially distributed reaction terms with a loacalized reaction at $\hat{x} = 0$. Nondimensional variables and parameters are introduced to formulate the scaling and simplify the analysis. For clarity, all solutions of the leading-order equations are displayed in dimensional as well as nondimensional form.

We introduce the following nondimensional variables,

$$T = \tilde{T}/\tilde{T}_*, \quad \rho = \tilde{\rho}_g/\tilde{\rho}_{go}, \quad P = \tilde{P}/\tilde{P}_o, \quad Y = \tilde{Y}/\tilde{Y}_o,$$
$$U = c_s\tilde{\rho}_{so}\tilde{u}/U_*, \quad V = c_g\tilde{\rho}_g(\tilde{v}_g - \tilde{u})/U_*, \quad \varphi = \phi/L, \quad \ell = l_{\mathrm{HTD}}/L. \tag{1.12}$$

where U represents the fuel-conversion rate, *i.e.* the amount of solid fuel passing through the reaction site, V represents the gas flux passing through the reaction site, and ℓ represents the as yet unknown position of the heat-transfer layer. Note that ℓ may be positive or negative. It is positive (negative) in the reaction-leading (trailing) structure. We also introduce the parameters

$$p = \frac{\tilde{P}_o}{g\tilde{\rho}_{go}L} \gg 1, \quad r = \frac{\tilde{\rho}_{go}c_g}{\tilde{\rho}_{so}c_s} \ll 1, \quad Le = \frac{\lambda}{D\tilde{\rho}_{go}c_g} \gg 1, \quad B = \frac{g\tilde{\rho}_{go}^2c_g}{\tilde{f}_+U_*},$$
$$q = \frac{\tilde{Q}}{c_s\tilde{T}_*}, \quad T_o = \frac{\tilde{T}_o}{\tilde{T}_*}, \quad F = \frac{\tilde{f}_-}{\tilde{f}_+}, \quad f = \frac{\tilde{f}}{\tilde{f}_+}, \quad \mu_o = \frac{\mu_g\tilde{Y}_o}{\mu}, \quad \delta = \frac{\mu c_g}{\tilde{Y}_oc_s},$$
$$W = \frac{\tilde{W}L\tilde{\rho}_{so}c_s}{U_*}, \quad E = \frac{\tilde{E}}{R\tilde{T}_*}, \quad \alpha = \frac{\tilde{\alpha}\lambda}{U_*^2}, \quad \varepsilon = \frac{\lambda}{LU_*} = \frac{l_C}{L} \ll 1. \tag{1.13}$$

The spatial and temporal variables are scaled as

$$x = \frac{\hat{x}}{L} = \frac{\tilde{x} + \phi(\tilde{t})}{L}, \quad t = \frac{U_*\tilde{t}}{L\tilde{\rho}_{so}c_s}. \tag{1.14}$$

The reference temperature $\tilde{T}_*$ is given by

$$\tilde{T}_* = \tilde{T}_o + \frac{\tilde{Q}/c_s}{|1 - \delta(1 + \mu_o)|}, \tag{1.15}$$

which we will show is the burning temperature for the stoichiometric mode of propagation. The reference heat capacity weighted solid-consumption rate U_* is given by

$$U_* = c_s\sqrt{\frac{2\lambda\tilde{\rho}_{so}K_oR\tilde{T}_*^2}{\tilde{E}\tilde{Q}}}\,\mathrm{e}^{-\frac{\tilde{E}}{2R\tilde{T}_*}}. \tag{1.16}$$

The nondimensional reaction rate W is

$$W = \tfrac{1}{2} q E \varepsilon^{-1} H(1-\eta) H(Y)\, \mathrm{e}^{E(1-1/T)}. \tag{1.17}$$

The nondimensional formulation of the system of equations is

$$(r\rho + 1 - \mu_o \delta \eta)\frac{\partial T}{\partial t} + \frac{\alpha}{\varepsilon}(T - T_o) + C\frac{\partial T}{\partial x} - \varepsilon \frac{\partial^2 T}{\partial x^2} = qW, \tag{1.18}$$

$$r\frac{\partial \rho}{\partial t} - \frac{\partial V}{\partial x} = \mu_o \delta W, \qquad r\frac{\partial \rho Y}{\partial t} - \frac{\partial}{\partial x}\left[VY + \frac{\varepsilon \rho}{Le}\frac{\partial Y}{\partial x}\right] = -\delta W, \tag{1.19–1.20}$$

$$\frac{\partial \eta}{\partial t} + U\frac{\partial \eta}{\partial x} = W, \tag{1.21}$$

$$p\frac{\partial P}{\partial x} - \frac{f}{B}\left(\frac{V}{\rho} + Ur\right) - \rho = 0, \qquad P = \rho T / T_o, \tag{1.22–1.23}$$

where

$$C = (1 - \mu_o \delta \eta)U - V. \tag{1.24}$$

The boundary conditions are

$$\text{at } x = \varphi - 1\text{:} \quad P = 1 - \frac{1}{p}, \quad \frac{\partial T}{\partial x} = 0, \quad \frac{\partial Y}{\partial x} = 0, \quad \eta = 0,$$

$$\text{at } x = \varphi\text{:} \quad P = 1, \quad T = T_o, \quad Y = 1. \tag{1.25}$$

We simplify the model by employing the assumptions stated previously and restated here in terms of the nondimensional parameters of the problem. The resulting system is solved for the temperature T, degree of solid conversion η, gass mass flux V, oxidizer mass fraction Y, and fuel consumption rate U. The assumption that the hydrostatic pressure is much less than ambient pressure, $g\tilde{\rho}_{go}L \ll \tilde{P}_o$, implies that $p \gg 1$. The assumption that $\tilde{v}_g \gg \tilde{u}$ can be stated in terms of the nondimensional parameters as $r \ll 1$ and $B = O(1)$. The condition $r \ll 1$ states that the initial density of gas is much less than the density of the solid. We note that it implies that the time derivative terms in (1.19) and (1.20) are negligible. It also implies that the effective Lewis number $Le \gg 1$. For example, even for a very porous material such as polyeurethane foam, with a void fraction which exceeds 90%, using the data in [20, 21], we estimate an effective Lewis number of 60. The condition $B/r \gg 1$ corresponds to highly permeable samples and $B = O(1)$ ensures significant conversion of the solid. The condition that the scale of the combustion layer is much less than the length of the sample is stated as $\varepsilon \ll 1$. We proceed to find a leading-order model for $p \gg 1, r \ll 1$ and $Le \gg 1$. In this model we retain the small parameter ε. Employing this model, we describe solutions that vary on the slow-time scale εt.

First, we consider the momentum equation (Darcy's Law) (1.6) to derive an integral relation between the gas flux induced by buoyancy forces and an appropriate average temperature in the sample. This relation will replace the momentum equation in our system. Then, we replace the spatially distributed reaction terms with jump conditions across the reaction site $x = 0$.

Finally, we derive a relation between the position of the heat-transfer layer ℓ, and that of the combustion layer, φ. In subsequent sections, we describe solutions to this system.

For $p \gg 1$, (1.22) implies that the pressure is constant in space, so that by the equation of state (1.23), density is inversely proportional to temperature,

$$\rho \cong T_o/T. \tag{1.26}$$

The momentum equation (1.22) can be integrated across the sample to obtain a relation between V and an average temperature. Using (1.26) and integrating (1.22) across the entire sample, we obtain

$$\int_{\varphi-1}^{\varphi} \frac{fVT}{T_o}\,\mathrm{d}x = B\int_{\varphi-1}^{\varphi}\left(1-\frac{T_o}{T}\right)\mathrm{d}x, \tag{1.27}$$

which is a relation between the buoyancy-driven mass flux V, and spatial averages of the temperature and its inverse. The right-hand side of the relation represents the buoyant force which increases with gravity (through B) and with temperature. The left-hand side represents the resistance or frictional forces. Equation (1.27) will be used to replace Darcy's Law (1.6) in our model.

We now proceed to replace the reaction zone by a front, a process known as large-activation-energy asymptotics. The reaction term in the equations is replaced by jump conditions across the front. On the scale of the combustion layer, the large activation energy implies that the reaction zone is thin. Using large activation energy asymptotics, we replace the spatially distributed reaction terms in equations (1.18)–(1.24) with a localized reaction at $x = 0$. Replacing the reaction terms with conditions at $x = 0$, we obtain equations without the reaction terms which are valid away from $x = 0$, and jump conditions across the front given by

$$[T]_o = 0, \quad [\rho]_o = 0, \tag{1.28}$$

$$\varepsilon\left[\frac{\partial T}{\partial x}\right]_o = -qU[\eta]_o, \quad [V]_o = -\mu_o\delta U[\eta]_o, \quad [VY]_o = \delta U[\eta]_o, \tag{1.29}$$

where $[z(x)]_o = z(0+) - z(0-)$ denotes the jump in the quantity z across the front. In general, $[z(x)]_w = z(x = w_+) - z(x = w_-)$.

We derive two additional conditions from integral relations obtained by integrating Equation (1.18) in the reaction zone,

$$\left(\frac{\partial T}{\partial x}\right)^2\Bigg|_{x=0_-} = \frac{q^2E}{\varepsilon^2}\int_{T_o}^{T_b} H(Y)\,\mathrm{e}^{E(1-1/T)}\,\mathrm{d}T, \tag{1.30}$$

$$\left(\frac{\partial T}{\partial x}\right)^2\Bigg|_{x=0_+} = \frac{q^2E}{\varepsilon^2}\int_{T_o}^{T_b} H(1-\eta)\,\mathrm{e}^{E(1-1/T)}\,\mathrm{d}T. \tag{1.31}$$

The integrals depend on the reactant concentrations and, in particular, the temperature where the reaction rate is affected by reactant concentration. We define

$$\xi_1 = I_R^{-1}\int_{T_o}^{T_b} H(Y)\,\mathrm{e}^{E(1-1/T)}\,\mathrm{d}T, \tag{1.32}$$

and

$$\xi_2 = I_R^{-1} \int_{T_o}^{T_b} H(1-\eta)\, \mathrm{e}^{E(1-1/T)}\, \mathrm{d}T, \tag{1.33}$$

where the integral I_R is

$$I_R \equiv \int_{T_o}^{T_b} \mathrm{e}^{E(1-1/T)}\, \mathrm{d}T \cong \frac{T_b^2}{E}\, \mathrm{e}^{E(1-1/T_b)}, \tag{1.34}$$

and the asymptotic evaluation shown in Equation (1.34) holds for narrow reaction zones (*i.e.* for asymptotically large Zeldovich Number $Z = \tilde{E}(\tilde{T}_* - \tilde{T}_o)/R\tilde{T}_*^2 = E(1 - T_o/T) \gg 1$). The conditions (1.30) and (1.31) become

$$\left(\frac{\partial T}{\partial x}\right)^2 \bigg|_{x=0_-} = \left(\frac{qT_b}{\varepsilon}\right)^2 \xi_1\, \mathrm{e}^{E(1-1/T_b)}, \tag{1.35}$$

$$\left(\frac{\partial T}{\partial x}\right)^2 \bigg|_{x=0_+} = \left(\frac{qT_b}{\varepsilon}\right)^2 \xi_2\, \mathrm{e}^{E(1-1/T_b)}. \tag{1.36}$$

The variables ξ_1 and ξ_2 are as yet unknown, but we now argue that

$$(1-\xi_1)Y_- = 0, \quad (1-\xi_2)(1-\eta_+) = 0, \tag{1.37–1.38}$$

and $\xi_1, \xi_2 \leqslant 1$ where Y_- denotes the value of Y immediately ahead of the front and η_+ denotes the value of η immediately behind the front. The definitions (1.32)–(1.34) ensure that $\xi_1, \xi_2 \leq 1$, with $\xi_1 = 1$ if and only if $H(Y) = 1$ ahead of the front and $\xi_2 = 1$ if and only if $H(1-\eta) = 1$ behind the front. Thus, $\xi_1 < 1$ when the reaction terminates due to lack of oxygen $(Y_- = 0)$ and $Y_- > 0$ ensures $\xi_1 = 1$. Similarly, $\xi_2 < 1$ when the reaction terminates due to lack of solid fuel $(\eta_+ = 1)$ and $\eta_+ < 1$ ensures $\xi_2 = 1$.

Equations (1.28), (1.29), and (1.35)–(1.38) are conditions for quantities at the reaction site which allow us to match the solutions determined on either side of the front.

We now proceed to a discussion of the location of the combustion and heat-transfer layers. The reaction zone lies at $x = 0$, within the combustion layer. On the scale of the sample, the position of the combustion layer can thus be taken to be $x = 0$. The portion of the sample that has been burned is measured by φ. By determining φ, we thus determine the position of the combustion layer in laboratory coordinates. Furthermore, a relation between the position of the heat-transfer layer $x = \ell$ and the burned portion of the sample φ can be obtained by examination of the energy equation (1.18) in the adiabatic case. We now proceed to find this relation. This derivation closely follows that presented in [6, 14] for the forced-flow case. The non-adiabatic case, when heat losses are significant, does not exhibit a heat-transfer layer, so such an analysis is not needed.

We consider (1.18), using a coordinate system chosen so that the burned region of the sample has a fixed length. This time-dependent spatial coordinate $\zeta = x/\varphi$ also ensures that the heat-transfer layer does not move with time. Solving for the position ζ_{cr} of the heat-transfer layer and writing this expression in our original coordinates we obtain a relation between ℓ and φ.

To leading order for $r \ll 1$ and for $\alpha = 0$, Equation (1.18) can be written in the new coordinate system as

$$\varphi^2(1-\mu_o\delta\eta)\frac{\partial T}{\partial t}+\varphi((1-\mu_o\delta\eta)(1-\zeta)U-V)\frac{\partial T}{\partial \zeta}-\varepsilon\frac{\partial^2 T}{\partial \zeta^2}=0. \tag{1.39}$$

We seek stationary (time-independent) solutions of (1.39) in the moving coordinate system ζ, and thus neglect the time-derivative term, to obtain

$$\varphi((1-\mu_o\delta\eta)(1-\zeta)U-V)\frac{\partial T}{\partial \zeta}-\varepsilon\frac{\partial^2 T}{\partial \zeta^2}=0. \tag{1.40}$$

Boundary conditions for the temperature in this domain are

$$\text{at } \zeta=0\text{:}\quad T=T_b; \qquad \text{at } \zeta=1\text{:}\quad T=T_o, \tag{1.41}$$

For $\varepsilon \ll 1$ we have a singular-perturbation problem. The outer solution is given by $T = T_b$ for $0 < \zeta < \zeta_{\text{cr}}$, and $T = T_o$ for $\zeta_{\text{cr}} < \zeta < 1$. The solution exhibits an interior layer (the heat-transfer layer) at $\zeta = \zeta_{\text{cr}}$. We can determine the location ζ_{cr} by examining the coefficients of (1.40). The equation ensures that $\partial T/\partial\zeta = O(\varepsilon)$, unless its coefficient is zero. The position of ζ_{cr} is determined as that value of ζ for which the coefficient is zero. Thus,

$$\zeta_{\text{cr}}=\frac{\ell}{\varphi}=1-\frac{V}{U(1-\mu_o\delta\eta)}. \tag{1.42}$$

In this expression, V and η should be evaluated at the heat-transfer layer. We will show that for the reaction-leading structure, at the heat-transfer layer, $\eta = 1$ and we denote $V = V_+$, so that,

$$\ell=\varphi\left(1-\frac{V_+}{U(1-\mu_o\delta)}\right). \tag{1.43}$$

For the reaction-trailing structure, we denote the values at the heat-transfer layer as $\eta = \eta_b$ and $V = V_-$, so that,

$$\ell=\varphi\left(1-\frac{V_-}{U(1-\mu_o\delta\eta_b)}\right). \tag{1.44}$$

Temperature varies in the heat-transfer layer from the burning temperature to the initial temperature. On the scale of the sample, this is a jump in temperature. Other variables are continuous across the layer, so we impose a single jump condition at the position of the heat-transfer layer $x = \ell$,

$$[T]_\ell \equiv T|_{\ell+} - T|_{\ell-} = -(T_b - T_o)C/|C|, \tag{1.45}$$

where the term $C/|C|$ is positive or negative, depending on whether the solution structure is reaction-leading or trailing.

We now summarize our assumptions and the simplified model that results from these assumptions. We have replaced the reaction terms by jump conditions at the front. We have used the assumptions $p \gg 1$, $r \ll 1$, and $Le \gg 1$ to obtain leading-order equations, replacing

the momentum equation with an appropriately derived integral relation. For now, we retain the small parameter ε in the equations. In subsequent sections, we show that ε determines the time scale upon which the solutions depend, so that $\varepsilon \ll 1$ corresponds to slowly varying waves. Density decouples from the equations as it is slaved to temperature by the equation of state and the fact that the pressure is essentially constant. For simplicity of exposition, we drop the equation of state and the variable ρ from consideration.

The model we consider is thus given by

$$(1-\mu_o\delta\eta)\frac{\partial T}{\partial t}+\frac{\alpha}{\varepsilon}(T-T_o)+C\frac{\partial T}{\partial x}-\varepsilon\frac{\partial^2 T}{\partial x^2}=0, \tag{1.46}$$

$$\frac{\partial V}{\partial x}=0, \qquad \frac{\partial VY}{\partial x}=0, \qquad \frac{\partial \eta}{\partial t}+U\frac{\partial \eta}{\partial x}=0, \tag{1.47–1.49}$$

$$B\int_{\varphi-1}^{\varphi}\left(1-\frac{T_o}{T}\right)\,\mathrm{d}x=\int_{\varphi-1}^{\varphi}\frac{fVT}{T_o}\,\mathrm{d}x, \tag{1.50}$$

where

$$C=U(1-\mu_o\delta\eta)-V. \tag{1.51}$$

The conditions at the reaction site $x=0$ are

$$[T]_o=0, \qquad [\rho]_o=0, \tag{1.52}$$

$$\varepsilon\left[\frac{\partial T}{\partial x}\right]_o=-qU[\eta]_o, \qquad [V]_o=-\mu_o\delta U[\eta]_o, \qquad [VY]_o=\delta U[\eta]_o, \tag{1.53}$$

$$\left(\frac{\partial T}{\partial x}\right)^2\Big|_{x=0_-}=\left(\frac{qT_b}{\varepsilon}\right)^2\xi_1\,\mathrm{e}^{E(1-1/T_b)}, \qquad (1-\xi_1)Y_-=0, \tag{1.54–1.55}$$

$$\left(\frac{\partial T}{\partial x}\right)^2\Big|_{x=0+}=\left(\frac{qT_b}{\varepsilon}\right)^2\xi_2\,\mathrm{e}^{E(1-1/T_b)}, \qquad (1-\xi_2)(1-\eta_+)=0. \tag{1.56–1.57}$$

The jump condition at the heat-transfer layer at $x=\ell$ is

$$[T]_\ell=-(T_b-T_o)C/|c|, \tag{1.58}$$

where

$$\ell=\frac{\varphi C}{U(1-\mu_o\delta\eta)}=\varphi\left(1-\frac{V}{U(1-\mu_o\delta\eta)}\right), \tag{1.59}$$

and the boundary conditions are

$$\text{at } x=\varphi-1\text{:} \qquad \frac{\partial T}{\partial x}=0, \qquad \frac{\partial Y}{\partial x}=0, \qquad \eta=0, \tag{1.60}$$

$$\text{at } x=\varphi\text{:} \qquad T=T_o, \qquad Y=1. \tag{1.61}$$

Initial conditions are assumed to be sufficiently close to the wave solutions that the transient time is negligibly small. Thus, we discuss wave solutions which arise after transients have dissipated. The sample is initially cool at temperature T_o, and, while the temperature of the incoming gas is not necessarily T_o, we choose it to be so for ease of exposition.

We now proceed to derive solutions to this system for two cases depending on the relative lengths of the HTD, $l_{\rm HTD} = |\ell L|$, and the cooling length $l_\alpha = 2/(\sqrt{C^2+4\alpha} - |C|)$. In Section 2, we consider the case $l_{\rm HTD} \ll l_\alpha$, or adiabatic combustion in which heat losses can be neglected, because the temperature drops in the heat-transfer layer before heat losses can have an effect. Since $l_{\rm HTD}$ grows with time, these solutions are valid only for intermediate times, *i.e.* after the ignition process and before heat losses affect the wave structure. In Section 3, we consider sufficiently large $l_{\rm HTD}$ for heat losses to affect the structure. These solutions are valid in the long-time limit and are observed in sufficiently long samples. We require the samples to be sufficiently long for the combustion wave to be completely contained within the sample.

2. Adiabatic combustion

We now consider adiabatic combustion, that is, we consider the system (1.46)–(1.61) with $\alpha = 0$. As in the case of forced forward FC, we find two solution structures referred to as reaction-leading and reaction trailing. We further categorize solution within each structure as stoichiometric, if both of the reactants are completely consumed in the reaction, and kinetically controlled if either reactant remains after combustion.

We first examine the equations on the scale of the sample and consider the limit that the unburned portion of the sample is much longer than the length scales of both the heat-transfer layer and the combustion layer, $L-\phi \gg l_c, l_h$ or equivalently $\varepsilon \ll 1$. We look for quasi-steady solutions in which the profile changes only due to the relative motion of the layers. Thus, changes occur on the slow-time scale $\tau = \varepsilon t$. To leading order, the temperature is spatially piecewise constant with cool regions at the temperature T_o ahead of and behind the HTD. On this scale, the solution appears to have jumps in temperature at each end of the HTD. On smaller scales, these jumps are, in fact, layers (the combustion and heat-transfer layers). Time dependence arises only through φ and ℓ which change slowly as the reaction proceeds along the sample.

We examine the equations on the scale $X = x/\varepsilon$ of the combustion layer to determine the structure of the layers. The solutions depend on constants which are determined by the jump conditions at the reaction site. These conditions determine whether the solution structure is reaction-leading or reaction-trailing and we consider each separately. Rewriting (1.46)–(1.49) to reflect the adiabatic quasi-steady assumptions, which we verify for the solutions below, yields

$$C\frac{\partial T}{\partial X} - \frac{\partial^2 T}{\partial X^2} = 0, \qquad \frac{\partial Y}{\partial X} = 0, \qquad \frac{\partial V}{\partial X} = 0, \qquad \frac{\partial \eta}{\partial X} = 0, \tag{2.1–2.4}$$

$$C = U(1-\mu_o\delta\eta) - V. \tag{2.5}$$

Note that (2.3) and (2.4) ensure that C has no spatial variation. The solution of (2.1)–(2.4) for $X < 0$ is

$$\eta = 0, \qquad V = V_-, \tag{2.6}$$

$$T = T_o + (T_b - T_o)\,\mathrm{e}^{k_1 X}, \qquad Y = Y_-, \tag{2.7}$$

where $k_1 = \max(0, C)$. The solution for $X > 0$ is

$$\eta = \eta_b, \qquad V = V_+; \qquad T = T_o + (T_b - T_o)\,\mathrm{e}^{k_2 X}, \qquad Y = Y_+ = 1, \tag{2.8–2.9}$$

where $k_2 = \min(0, C)$. The coefficients k_1 and k_2 change form when C changes sign, because the structure of the solution changes from reaction-leading $(C > 0)$ to reaction-trailing $(C < 0)$. We first consider reaction-leading structures and then reaction-trailing.

2.1. Reaction-leading structure

Equations (2.6)–(2.9) and the conditions (1.52)–(1.59) determine the unknowns $T_b, U, V_+, V_-, C, \eta_b, \xi_1, \xi_2, \ell$ and Y_- in terms of φ. For the reaction-leading structure $(C > 0)$, the equations determining these quantities are

$$\xi_1 = C^2 (T_b - T_o)^2 T_b^{-2}\,\mathrm{e}^{E(1/T_b - 1)}, \tag{2.10}$$

$$\xi_2 = 0, \qquad (1 - \xi_1) Y_- = 0, \qquad (1 - \xi_2)(1 - \eta_b) = 0, \tag{2.11–2.13}$$

$$T_b = T_o + qU/C, \qquad V_+ = V_- - \mu_o \delta U, \qquad V_- = Y_- V_- + \delta U, \tag{2.14–2.16}$$

$$C = U - V_- = U(1 - \mu_o \delta) - V_+, \qquad \ell = \varphi \left(1 - \frac{V_+}{U(1 - \mu_o \delta)}\right), \tag{2.17–2.18}$$

$$V_+ [\varphi + \ell (T_b/T_o - 1) + F(1 - \varphi) V_- / V_+] = B\ell (1 - T_o/T_b). \tag{2.19}$$

Equations (2.11) and (2.13) show that the reaction-leading structure always leads to complete conversion $\eta_b = 1$. The solution is either stoichiometric or kinetically controlled, depending on whether $Y_- = 0$. Consider first the stoichiometric case, $Y_- = 0$, for which (2.16) yields

$$V_+ = \delta U. \tag{2.20}$$

Using (2.15), (2.18)–(2.20), we solve for V_+ in terms of φ as

$$V_+ = \frac{B\varphi \left(\frac{1 - \delta(1 + \mu_o)}{1 - \mu_0 \delta}\right) \left(\frac{T_b - T_o}{T_b}\right)}{F(1 + \mu_o) + \varphi \left[1 - F(1 + \mu_o) + \left(\frac{T_b}{T_o} - 1\right) \left(\frac{1 - \delta(1 + \mu_o)}{1 - \mu_o \delta}\right)\right]}, \tag{2.21}$$

where

$$T_b = T_o + \frac{q}{1 - \delta(1 + \mu_o)} = 1, \tag{2.22}$$

by (2.14)–(2.15), (2.20) and the scaling of the nondimensional temperature (1.15). In dimensional variables, (2.21) is

$$\tilde{\rho}_g (\tilde{v}_g - \tilde{u})_+ = \frac{g \tilde{\rho}_{go}^2 \phi \left(\frac{\tilde{T}_b - \tilde{T}_o}{\tilde{T}_b}\right) \left(\frac{\tilde{Y}_o c_s - \mu c_g - \mu_g \tilde{Y}_o c_g}{\tilde{Y}_o c_s - \mu_g \tilde{Y}_o c_g}\right)}{L \tilde{f}_- \left(1 + \frac{\mu_g \tilde{Y}_o}{\mu}\right) + \phi \left[\tilde{f}_+ - \tilde{f}_- \left(1 + \frac{\mu_g \tilde{Y}_o}{\mu}\right) + \left(\frac{\tilde{T}_b}{\tilde{T}_o} - 1\right) \left(\frac{\tilde{Y}_o c_s - \mu c_g - \mu_g \tilde{Y}_o c_g}{\tilde{Y}_o c_s - \mu_g \tilde{Y}_o c_g}\right)\right]}. \tag{2.23}$$

The dimensional burning temperature is

$$\tilde{T}_b = \tilde{T}_o + \frac{\tilde{Q}\tilde{Y}_o}{c_s\tilde{Y}_o - \mu c_g - \mu_g c_g \tilde{Y}_o}. \tag{2.24}$$

It can be seen that $\tilde{T}_b$ may exceed the value

$$\tilde{T}_b^{\text{ad}} = \tilde{T}_o + \frac{\tilde{Q}\tilde{Y}_o}{c_s\tilde{Y}_o + \mu c_g}, \tag{2.25}$$

which is the thermodynamic adiabatic combustion temperature of a stoichiometric mixture of porous solid and ambient gas. Thus, for upward buoyant FC, superadiabatic temperatures are attainable. From (2.14)–(2.17) the unknowns V_-, U, and C can be written in terms of V_+ as

$$V_- = V_+(1+\mu_o), \qquad U = V_+/\delta, \tag{2.26–2.27}$$

and (2.18) yields

$$C = V_+(\delta^{-1} - \mu_o - 1). \tag{2.28}$$

The position of the heat transfer layer ℓ is proportional to φ as

$$\ell = \varphi\left(1 - \frac{\delta}{1-\mu_o\delta}\right). \tag{2.29}$$

Temperature is constant in time; gas flux and propagation velocity increase (slowly) with φ. Figure 3 shows the change in propagation velocity with φ for a representative choice of parameter values. Rates of increase are higher for parameter values favoring flow (*e.g.* large F or small T_o). Propagation velocity and gas flux increase proportionally to gravitational forces. For sufficiently large gravitational forces, the flow becomes sufficiently large that oxidizer supply does not restrict the reaction and the wave switches from the stoichiometric mode to the kinetically controlled mode.

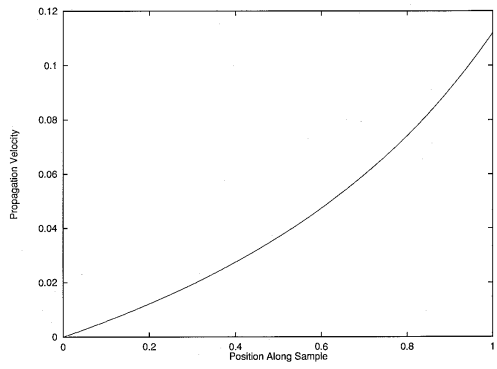

Figure 3. A typical trajectory of the propagation velocity as a reaction-leading, stoichiometric wave moves through the sample. Here, $T_o = 0{\cdot}2$, $\delta = 0{\cdot}486$, $E = 5$, $B = 1{\cdot}0$, $F = 1{\cdot}5$, and $\mu_o = 1{\cdot}05$.

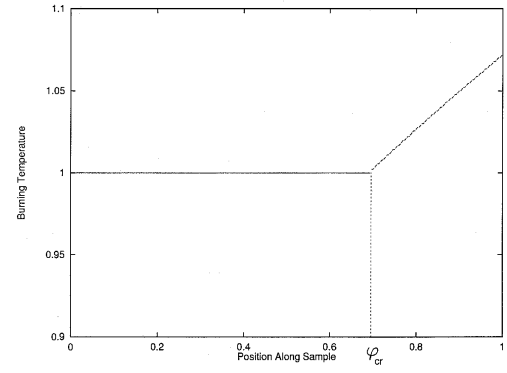

Figure 4. A typical trajectory of the burning temperature as a reaction-leading, stoichiometric wave becomes kinetically controlled, while moving through the sample. Here, $T_o = 0{\cdot}2$, $\delta = 0{\cdot}47$, $E = 5$, $B = 29$, $F = 2{\cdot}5$, and $\mu_o = 0{\cdot}5$.

Now consider the kinetically controlled case, $Y_- > 0$, where oxygen is supplied in sufficient quantities that kinetics limit the propagation of the wave and oxygen leaks through the reaction zone. For $Y_- > 0$, Equation (2.12) ensures that $\xi_1 = 1$. Equations (2.14) and (2.17) yield

$$\frac{U}{V_+} = \frac{1}{1 - \mu_o\delta - (q/(T_b - T_o))}, \tag{2.30}$$

which together with (2.10) allows us to formulate an implicit equation for T_b in terms of φ,

$$\frac{T_b}{q}\,\mathrm{e}^{\frac{1}{2}E(1-1/T_b)} = \frac{\varphi B \frac{q}{T_b(1-\mu_o\delta)}}{\left(1 - \mu_o\delta - \frac{q}{T_b - T_o}\right)\left[\varphi\left(1 + \frac{q}{T_o(1-\mu_o\delta)}\right) + F(1-\varphi)\left(\frac{1-\frac{q}{T_b-T_o}}{1-\mu_o\delta-\frac{q}{T_b-T_o}}\right)\right]}. \tag{2.31}$$

The dimensional relation is

$$\frac{\tilde{T}_b c_s}{\tilde{Q}}\sqrt{\frac{2\lambda\rho_{so}K_o R\tilde{T}_*^2}{\tilde{E}\tilde{Q}}}\,\mathrm{e}^{-\frac{\tilde{E}}{2R\tilde{T}_b}} = \frac{g\tilde{\rho}_{go}^2 c_g \phi \frac{\tilde{Q}}{\tilde{T}_b(c_s - \mu_g c_g)}}{\left(c_s - \mu_g c_g - \frac{\tilde{Q}}{\tilde{T}_b - \tilde{T}_o}\right)\left[\tilde{f}_+\phi\left(1 + \frac{q}{\tilde{T}_o(c_s+\mu_g c_g)}\right) + \tilde{f}_-(L-\phi)\left(\frac{c_s(\tilde{T}_b - \tilde{T}_o) - \tilde{Q}}{(\tilde{T}_b - \tilde{T}_o)(c_s - \mu_g c_g) - \tilde{Q}}\right)\right]}. \tag{2.32}$$

We can write the unknowns V_-, V_+, U, C, Y_- and ℓ in terms of T_b, using (2.14)–(2.18) as

$$U = \frac{T_b}{q}\,\mathrm{e}^{\frac{1}{2}E(1-1/T_b)}, \tag{2.33}$$

$$C = Uq/(T_b - T_o), \qquad V_- = U - C, \qquad V_+ = V_- - \mu_o\delta U, \tag{2.34–2.36}$$

$$Y_- = \frac{1 - \delta(1+\mu_o) - q/(T_b - T_o)}{1 - q/(T_b - T_o)}, \qquad \ell = \varphi\frac{q}{(T_b - T_o)(1 - \mu_o\delta)}. \tag{2.37–2.38}$$

The burning temperature T_b increases with φ. Figure 4 shows the change in T_b for representative parameter values. Rates of increase depend on F. For large F, the increase is quite strong and in complex reacting systems, such as smoldering, new reactions may become important. While transition to flaming is not described by the model, this sharp increase in T_b may indicate a mechanism of the transition. If so, this model predicts that for a given material, flaming would occur at a particular burned portion of the sample, independent of the length of the sample.

The transition between stoichiometric and kinetically controlled solutions occurs for parameter values such that equation (2.37) yields $Y_- = 0$. The temperature T_b corresponding to that point is identical to that in (2.22), *i.e.* $T_b = 1$, and plugging into (2.31) we obtain an expression for the critical burn portion $\varphi = \varphi_{\mathrm{cr}}$ for which the transition occurs,

$$\varphi_{\mathrm{cr}} = \frac{-F(1+\mu_o)}{1 + \frac{q}{T_o(1-\mu_o\delta)} - F(1+\mu_o) - \frac{q^2 B}{(1-\mu_o\delta)\delta}}. \tag{2.39}$$

For $\varphi_{\rm cr} > 1$, this transition will not occur during the burning of the sample. For $\varphi > \varphi_{\rm cr}$, the flux is sufficient to induce kinetically controlled waves. For $\varphi < \varphi_{\rm cr}$, the flux restricts the wave to stoichiometric propagation.

We now consider the reaction-trailing solution structure.

2.2. REACTION-TRAILING STRUCTURE

As for the reaction-leading structure, Equations (2.6)–(2.9) and the conditions (1.52)–(1.59) are sufficient to determine $T_b, U, V_+, V_-, C, \eta_b, Y_-, \ell, \xi_1$ and ξ_2 in terms of φ. The reaction-trailing structure occurs when $C < 0$ and the equations to determine the unknowns can be written,

$$\xi_1 = 0, \qquad \xi_2 = \frac{C^2(T_b - T_o)^2}{T_b^2}\, \mathrm{e}^{E(1/T_b - 1)}, \tag{2.40–2.41}$$

$$(1-\xi_1)Y_- = 0, \qquad (1-\xi_2)(1-\eta_b) = 0, \qquad T_b = T_o - qU\eta_b/C, \tag{2.42–2.44}$$

$$V_+ = V_- - \mu_o \delta U \eta_b, \qquad V_+ = \delta U \eta_b, \qquad C = U - V_-, \tag{2.45–2.47}$$

$$\ell = \max\left[\varphi - 1, \varphi\left(1 - \frac{V_-}{U}\right)\right], \qquad V_+ = \frac{-\ell B \frac{T_b - T_o}{T_b}}{\varphi + F\frac{V_-}{V_+}\left(-\ell\frac{T_b - T_o}{T_o} + 1 - \varphi\right)}. \tag{2.48–2.49}$$

Notice that $\ell < 0$ when $C < 0$. This means that the heat-transfer layer occurs ahead of the combustion layer and we have a reaction-trailing structure as supposed.

The restriction $\ell \geqslant \varphi - 1$ in (2.48) arises because the heat-transfer layer may leave the sample, while the reaction is still propagating. In that case, assuming the heated gas leaving the sample does not influence the buoyancy process, *e.g.* there is no chimney, we observe that the equations as derived are valid for $\ell = \varphi - 1$.

Equations (2.40) and (2.42) show that $Y_- = 0$ for the reaction-trailing structure. The solution is stoichiometric or kinetically controlled, depending on whether $\eta_b = 1$. We first consider the stoichiometric case $\eta_b = 1$, and obtain from (2.45) and (2.49) an expression for V_+ in terms of φ and ℓ as,

$$V_+ = \frac{-\ell B \frac{T_b - T_o}{T_b}}{F(1+\mu_o)\left(1 - \varphi - \ell\frac{T_b - T_o}{T_o} + \frac{\varphi}{F(1+\mu_o)}\right)}, \tag{2.50}$$

where

$$T_b = T_o + \frac{q}{\delta(1+\mu_o) - 1} = 1, \tag{2.51}$$

by (2.44), (2.47) and the scaling of temperature (1.15). The position of the heat-transfer layer ℓ, given by (2.45), (2.46) and (2.48), is

$$\ell = \max[\varphi - 1, \varphi(1 - \delta(1+\mu_o))]. \tag{2.52}$$

The dimensional relation is given by

$$\tilde{\rho}_g(\tilde{v}_g - \tilde{u})_+ = -\frac{g\tilde{\rho}_{go}^2\tilde{\ell}(\tilde{T}_b - \tilde{T}_o)/\tilde{T}_b}{\tilde{f}_-\left(1 + \frac{\mu_g\tilde{Y}_o}{\mu}\right)[L - \phi - \tilde{\ell}(\tilde{T}_b - \tilde{T}_o)/\tilde{T}_o] + \phi\tilde{f}_+}. \tag{2.53}$$

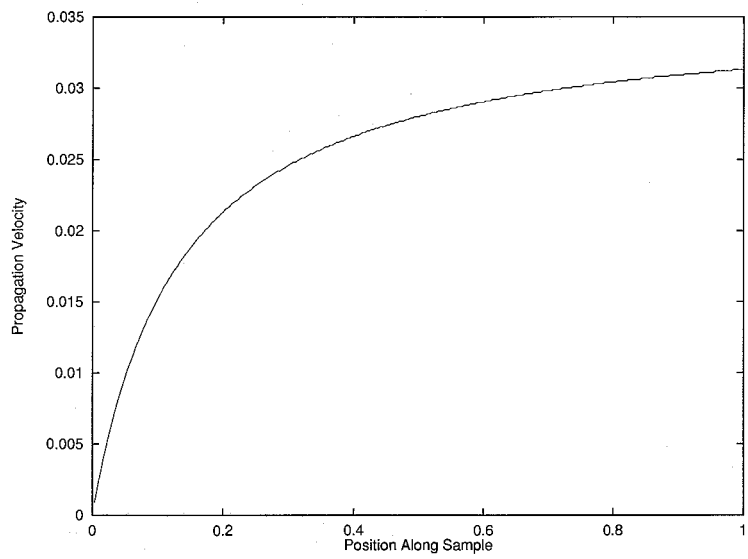

Figure 5. A typical trajectory of the propagation velocity as a reaction-trailing, stoichiometric wave moves through the sample. Here, $T_o = 0{\cdot}2$, $\delta = 1{\cdot}5$, $E = 5$, $B = 1{\cdot}0$, $F = 1{\cdot}0$, and $\mu_o = 1{\cdot}0$.

We can write the unknowns V_-, U, and C, using (2.45)–(2.47) in terms of V_+, as

$$V_- = V_+(1+\mu_o), \qquad U = V_+/\delta, \qquad C = U(1-\delta(1+\mu_o)). \tag{2.54–2.56}$$

As for the reaction-leading structure, the burning temperature does not vary in the stoichiometric mode. The gas flux and propagation velocity increase with φ. The curve (Figure 5) showing U *vs.* φ is concave downward, indicating that U will increase at a slower rate as φ gets larger. This in contrast to the reaction-leading structure where the rate of increase accelerated with φ. Values of F, and T_o, which favor flow yield a sharper bend in the curve. Much of the increase occurs for small φ and U is relatively constant for larger φ.

The kinetically controlled case occurs when $\eta_b < 1$ and by (2.43) $\xi_2 = 1$. Here fuel leakage occurs because it is cooled by the incoming gas before it can burn. In a similar manner to the reaction-leading structure, using (2.41), (2.44), (2.46) and (2.49), we obtain an implicit expression to determine T_b,

$$F(1+\mu_o)\delta\frac{T_b}{q}\,\mathrm{e}^{\frac{1}{2}E(1-1/T_b)} = \frac{-\ell B(T_b-T_o)/T_b}{1-\ell(T_b-T_o)/T_o+\varphi(F^{-1}(1+\mu_o)^{-1}-1)}, \tag{2.57}$$

where

$$\ell = \max\left[\varphi-1, \varphi\frac{q}{q-\delta(1+\mu_o)(T_b-T_o)}\right]. \tag{2.58}$$

The dimensional version of this expression is

$$\sqrt{\frac{2\lambda\rho_{so}K_oR\tilde{T}_*^2}{\tilde{E}\tilde{Q}}}\,\frac{\tilde{T}_bc_s}{\tilde{Q}}\,\mathrm{e}^{-\frac{\tilde{E}}{2R\tilde{T}_b}}$$

$$= -\frac{g\tilde{\rho}_{go}^2\tilde{\ell}(\tilde{T}_b - \tilde{T}_o)/\tilde{T}_b}{\tilde{f}_-(\mu c_g/\tilde{Y}_o + \mu_g c_g)[L - \tilde{\ell}(\tilde{T}_b - \tilde{T}_o)/T_o] + \phi\mu c_g/\tilde{Y}_o \cdot (\tilde{f}_+ - \tilde{f}_-(1 + \mu_g\tilde{Y}_o/\mu))}. \tag{2.59}$$

The unknowns V_+, V_-, U, η_b and C can be written by means of (2.41), and (2.44)–(2.47) in terms of T_b as

$$V_+ = \delta\frac{T_b}{q}\,\mathrm{e}^{\frac{1}{2}E(1-1/T_b)}, \qquad V_- = V_+(1+\mu_o), \qquad C = -\frac{V_+}{\delta}\frac{q}{T_b - T_o} \tag{2.60–2.62}$$

$$U = V_+\delta^{-1}(\delta(1+\mu_o) - q/(T_b - T_o)) \tag{2.63}$$

$$\eta_b = [\delta(1+\mu_o) - q/(T_b - T_o)]^{-1} \tag{2.64}$$

The transition between stoichiometric and kinetically controlled solutions occurs for parameter values such that (2.64) yields $\eta_b = 1$. This condition is identical to (2.51), so that plugging into (2.57) we obtain an expression for the critical burned portion $\varphi = \varphi_{\text{cr}}$ where the transition occurs,

$$\varphi_{\text{cr}} = \frac{\delta F(1+\mu_o)}{\delta(F(1+\mu_o) - 1) + (\delta(1+\mu_o) - 1)[Bq(1-T_o) - \delta F(1+\mu_o)(1/T_o - 1)]}. \tag{2.65}$$

For $\varphi_{\text{cr}} > 1$, this transition will not occur during the burning of the sample. For $\varphi < (>)\varphi_{\text{cr}}$, the solution is stoichiometric (kinetically) controlled.

We note that solutions will not change from reaction-trailing to reaction leading during propagation. The expressions for the flux-weighted heat capacity C in each solution show that as φ increases C does not change sign.

By examining a change in the initial parameters of the problem, however, we see that the model predicts whether reaction-trailing or leading solutions will be obtained. First note that the kinetically controlled solutions do not allow changes in the sign of C. Thus, near the boundary between regions, only stoichiometric solutions will be relevant. For stoichiometric solutions, (2.28) and (2.56) show that the critical parameter values are

$$\delta(1+\mu_o) = 1. \tag{2.66}$$

For $\delta(1+\mu_o) < (>)1$, reaction-leading (trailing) solutions occur. This matches the result obtained for forced FC. The analysis in [6, 14] shows that the boundary is independent of incoming gas flux, so it is not surprising that buoyancy retains this feature.

3. External heat losses

We now move to a treatment of external heat losses from the system. Heat losses to the external environment become important when the distance between the combustion layer and the heat transfer layer is sufficiently long that heat lost to the external environment is large compared to the heat transferred to the fresh reactants in the heat-transfer layer for the adiabatic case. Reaction-leading structure waves occur when the incoming gas cools the burned region, while

reaction-trailing structure waves occur when the fresh fuel cools the gas which has been heated while passing through the reaction site.

In contrast, when heat losses are important, the change in temperature at the heat-transfer layer is not significant. The temperature profile consists of a high-temperature region near the combustion layer which decays exponentially outside that region. The temperature decreases due to heat losses before the heat-transfer layer is reached. We assume that the decay is sufficiently fast that the temperature at each end of the sample is approximately the ambient temperature *i.e.* $L \gg l_\alpha$. Thus, the wave is completely contained within the sample.

We again find two solution structures which we label reaction-leading and reaction-trailing, as for the adiabatic case, according to the sign of the effective heat capacity C of the material passing through the reaction site. We look for quasi-steady solutions varying on the scale of the slow time $\tau = \varepsilon t$. Time dependence arises only through φ which changes slowly as the reaction proceeds through the sample. We examine (1.46)–(1.61) on the scale $X = x/\varepsilon$ of the combustion layer to obtain

$$\alpha(T - T_o) + C\frac{\partial T}{\partial X} - \frac{\partial^2 T}{\partial X^2} = 0, \tag{3.1}$$

$$\frac{\partial Y}{\partial X} = 0, \qquad \frac{\partial V}{\partial X} = 0, \qquad \frac{\partial \eta}{\partial X} = 0, \qquad C = U(1 - \mu_o \delta\eta) - V. \tag{3.2–3.5}$$

Note that (3.3) and (3.4) ensure that C has no spatial variation. The solution of (3.1)–(3.4) for $X < 0$ is

$$\eta = 0, \qquad V = V_-; \qquad T = T_o + (T_b - T_o)\,\mathrm{e}^{k_1 X}, \qquad Y = Y_-, \tag{3.6–3.7}$$

where

$$k_1 = \tfrac{1}{2}(C + \sqrt{C^2 + 4\alpha}) > 0. \tag{3.8}$$

The solution for $X > 0$ is

$$\eta = \eta_b, \qquad V = V_+; \qquad T = T_o + (T_b - T_o)\,\mathrm{e}^{k_2 X}, \qquad Y = 1, \tag{3.9–3.10}$$

where

$$k_2 = \tfrac{1}{2}(C - \sqrt{C^2 + 4\alpha}) < 0. \tag{3.11}$$

Evaluating the integrals in Equation (1.50) for the case $\varepsilon \ll 1$, we obtain

$$V_+\varphi + FV_-(1 - \varphi) = \varepsilon B \alpha^{-1} \log(T_b/T_o)\sqrt{C^2 + 4\alpha}. \tag{3.12}$$

For significant flux to occur, we must have $\varepsilon B = O(1)$. For $B = O(1)$, the model predicts extinction when heat losses are significant. This agrees with [11] who note that under normal gravity conditions, heat losses must be reduced for combustion to occur. In addition, it predicts that by increasing $B = g\tilde{\rho}_{go}^2 c_g / f_+ U_*$, we may attain smolder propagation, even with significant heat losses. The resistance and frictional forces act over the entire sample, while buoyancy can only be driven by the heated portion of the sample. Since external heat loss

reduces the size of the heated portion of the sample, $B = O(\varepsilon^{-1})$ is required for propagation. We retain the coefficient εB in our leading-order analysis, assuming that it is an $O(1)$ quantity.

Equations (3.6)–(3.12) and conditions (1.52)–(1.57) are sufficient to determine the unknowns $T_b, U, V_-, V_+, C, \eta_b, Y_-, \xi_1$ and ξ_2 in terms of φ. The equations determining these unknowns for both reaction-leading and trailing solutions can be written

$$\xi_1 = \frac{(C + \sqrt{C^2 + 4\alpha})^2 (T_b - T_o)^2}{4q^2 T_b^2} \, \mathrm{e}^{E(1/T_b - 1)}, \tag{3.13}$$

$$\xi_2 = \frac{(C - \sqrt{C^2 + 4\alpha})^2 (T_b - T_o)^2}{4q^2 T_b^2} \, \mathrm{e}^{E(1/T_b - 1)}, \tag{3.14}$$

$$(1 - \xi_1) Y_- = 0, \qquad (1 - \xi_2)(1 - \eta_b) = 0, \tag{3.15–3.16}$$

$$T_b = T_o + \frac{qU\eta_b}{\sqrt{C^2 + 4\alpha}}, \tag{3.17}$$

$$V_+ = V_- - \mu_o \delta U \eta_b, \qquad V_+ = V_- Y_- + \delta U \eta_b, \tag{3.18–3.19}$$

$$C = U - V_-, \qquad \frac{V_+}{U\eta_b} = \frac{\frac{\varepsilon B}{\alpha} \frac{q}{T_b - T_o} \log(T_b/T_o)}{\varphi + F(V_-/V_+)(1 - \varphi)}. \tag{3.20–3.21}$$

Traveling waves are found as a special case of these slowly varying waves. The slow variation arises due to the change in φ with time in (3.21). In the special case when $FV_- = V_+$, the φ dependence drops out and a traveling wave results. The condition $FV_- = V_+$ states that frictional forces remain unchanged by the reaction. For example, when the friction coefficient is unchanged by the reaction $(F = 1)$, and no net production of gas occurs in the reaction $(\mu_g = 0)$, traveling waves are expected.

We note that (3.13) and (3.14) show $\xi_1 \neq \xi_2$ so that the physical restriction $\xi_1, \xi_2 \leqslant 1$ implies that both $\eta_b = 1$ and $Y_- = 0$ cannot occur. At most one reactant can leak through the reaction zone. In the reaction-leading (trailing) structure, $\xi_1 > (<) \xi_2$, so that $\eta_b = 1 (Y_- = 0)$. We first consider reaction-leading structures and then reaction-trailing structures.

3.1. Reaction-leading structure

For the reaction-leading structure, $C > 0$ and $\xi_2 < \xi_1 \leqslant 1$ so that (3.16) yields $\eta_b = 1$. As with the adiabatic solutions, reaction-leading structures cause complete conversion of the fuel.

Stoichiometric $(Y_- = 0)$ and kinetically limited $(Y_- > 0)$ cases arise, depending on the value of Y_-. We discuss the stoichiometric case first. When $Y_- = 0$, Equation (3.19) shows that

$$V_+ = \delta U. \tag{3.22}$$

Combination with (3.17) and (3.21) gives an implicit expression for T_b in terms of φ,

$$\frac{\varepsilon B}{\alpha} \frac{q}{T_b - T_o} \log(T_b/T_o) = \delta[\varphi + F(1 + \mu_o)(1 - \varphi)]. \tag{3.23}$$

The dimensional version of the expression is

$$\tilde{\alpha}[\phi\tilde{f}_+ + \tilde{f}_-(1+\mu_g\tilde{Y}_o/\mu)(L-\phi)] = \frac{g\tilde{\rho}_{go}^2\tilde{Q}}{\tilde{T}_b-\tilde{T}_o}\log(\tilde{T}_b/\tilde{T}_o) \tag{3.24}$$

The unknowns U, V_-, C are given by (3.17), (3.18) and (3.20) in terms of T_b by

$$U^2 = \frac{4\alpha}{q^2/(T_b-T_o)^2 - (1-\delta(1+\mu_o))^2}, \tag{3.25}$$

$$V_- = U\delta(1+\mu_o), \qquad C = U(1-\delta(1+\mu_o)). \tag{3.26–3.27}$$

Notice that the burning temperature T_b and, in turn, the wave structure do not depend on the kinetic parameters K_o and $\tilde{E}$. Reactant supply determines the propagation of the wave in the stoichiometric case. Kinetically limited solutions occur when $\xi_1 = 1$. Equation (3.13) gives C as a function of T_b,

$$C = \frac{q^2T_b^2(T_b-T_o)^{-2}\,\mathrm{e}^{E(1-1/T_b)} - \alpha}{qT_b(T_b-T_o)^{-1}\,\mathrm{e}^{\frac{1}{2}E(1-1/T_b)}}. \tag{3.28}$$

Equations (3.18) and (3.21) yield

$$\frac{V_+}{U} = J(T_b) \equiv \frac{\frac{\varepsilon B}{\alpha}\frac{q}{T_b-T_o}\log(T_b/T_o) - \mu_o\delta F(1-\varphi)}{F+(1-F)\varphi}, \tag{3.29}$$

so that (3.17), (3.18) and (3.20) combine to give an implicit expression for T_b in terms of φ:

$$\left(\frac{q}{T_b-T_o}\right)\frac{q^2T_b^2(T_b-T_o)^{-2}\,\mathrm{e}^{E(1-1/T_b)} - \alpha}{q^2T_b^2(T_b-T_o)^{-2}\,\mathrm{e}^{E(1-1/T_b)} + \alpha} = 1-\mu_o\delta - J(T_b). \tag{3.30}$$

The dimensional form of this relation is

$$\left(\frac{\tilde{Q}}{\tilde{T}_b-\tilde{T}_o}\right)\frac{(\tilde{Q}\tilde{T}_b)^2 2\lambda\rho_{so}K_oR\tilde{T}_*^2\,\mathrm{e}^{-\tilde{E}/(R\tilde{T}_b)} - \tilde{\alpha}\lambda\tilde{E}\tilde{Q}c_s^2(\tilde{T}_b-\tilde{T}_o)^2}{(\tilde{Q}\tilde{T}_b)^2 2\lambda\rho_{so}K_oR\tilde{T}_*^2\,\mathrm{e}^{-\tilde{E}/(R\tilde{T}_b)} + \tilde{\alpha}\lambda\tilde{E}\tilde{Q}c_s^2(\tilde{T}_b-\tilde{T}_o)^2}$$

$$= c_s - \mu_g c_g - \frac{g\tilde{\rho}_{go}^2c_g\tilde{Q}\tilde{\alpha}^{-1}(\tilde{T}_b-\tilde{T}_o)^{-1}\log\left(\frac{\tilde{T}_b}{\tilde{T}_o}\right) - \mu_g c_g\tilde{f}_-(L-\phi)}{L\tilde{f}_- + \phi(\tilde{f}_+ - \tilde{f}_-)}. \tag{3.31}$$

The unknowns U, V_+, V_-, and Y_- are then given by (3.18)–(3.21) as

$$U = \frac{C}{1-\mu_o\delta - J(T_b)}, \tag{3.32}$$

$$V_+ = UJ(T_b), \qquad V_- = V_+ + \mu_o\delta U, \qquad Y_- = \frac{J(T_b)-\delta}{J(T_b)+\mu_o\delta}. \tag{3.33–3.35}$$

Notice that for $Y_- > 0$ we must have $J(T_b) > \delta$. For each set of parameters, we must use (3.30) to determine the potential solution for T_b and then test it for $J(T_b) > \delta$ to see if the solution exists.

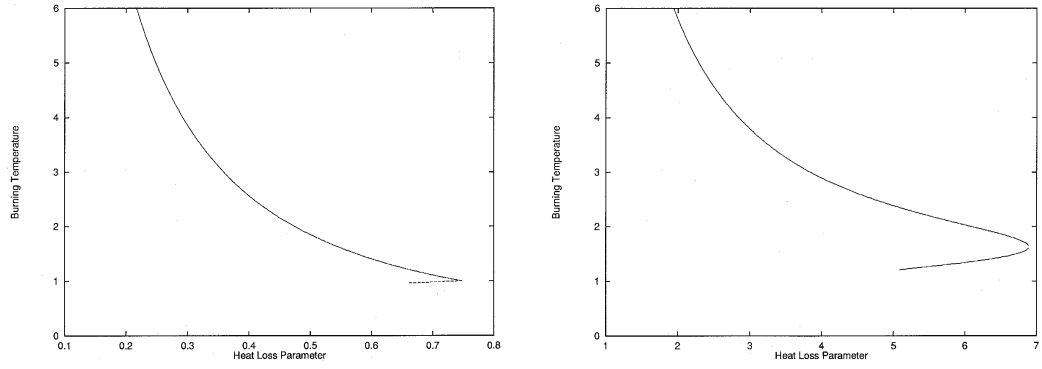

Figure 6. Burning Temperature at the middle of the sample as a function of the heat-loss parameter for reaction-leading structure solutions. In (a) only kinetically controlled solutions exist and extinction occurs for large α. In (b) Stoichiometric (solid) and Kinetically-Controlled (dashed) solutions both appear near the extinction point, extinction occurs at the boundary between the two. Here, $T_o = 0{\cdot}2, E = 5, \phi = 0{\cdot}5, \mu_o = 0{\cdot}01$, and for (a) $\delta = 0{\cdot}46, \varepsilon B = 2{\cdot}7$, and $F = 0{\cdot}5$. While for (b) $\delta = 0{\cdot}86, \varepsilon B = 0{\cdot}4$, and $F = 1{\cdot}0$.

Extinction occurs in the kinetically controlled mode for large α (see Figure 6a). In some cases, the stoichiometric mode exists near the extinction point, but extinction does not occur in the stoichiometric mode. It occurs at the boundary between stoichiometric and kinetically controlled solutions (see Figure 6b). The burning temperature moves smoothly to a critical value as α moves toward the extinction value $\alpha_{\rm cr}$. This extinction limit is similar in nature to that seen in many combustion problems for which heat losses are considered.

As α decreases, T_b, U and V_+ all increase dramatically. The reduction in heat loss not only allows higher temperatures, but these higher temperatures and longer heated regions cause buoyancy to bring in more gas which further increases the reaction rate and temperature. This feedback allows dramatic increases in burning rates and also allows combustion to continue for long periods without external intervention.

3.2. REACTION-TRAILING STRUCTURE

For the reaction-trailing structure, $C < 0$ and $\xi_1 < \xi_2 \leqslant 1$ so that (3.15) yields $Y_- = 0$. As with the adiabatic solutions, reaction-trailing structure causes all oxidizer to be consumed.

Stoichiometric $(\eta_b = 1)$ and kinetically limited $(\eta_b < 1)$ cases arise, depending on the value of η_b. The stoichiometric case has the same formulas for its solution as the reaction-leading stoichiometric case (3.22)–(3.27). The solutions differ only in that C becomes negative when $\delta(1 + \mu_o) > 1$. The boundary between stoichiometric reaction-leading and stoichiometric reaction-trailing solutions is

$$\delta(1 + \mu_o) = 1. \tag{3.36}$$

Kinetically limited solutions occur when $\xi_2 = 1$. Equation (3.14) gives C as a function of T_b,

$$-C = \frac{q^2 T_b^2 (T_b - T_o)^{-2}\, \mathrm{e}^{E(1-1/T_b)} - \alpha}{q T_b (T_b - T_o)^{-1}\, \mathrm{e}^{\frac{1}{2}E(1-1/T_b)}}. \tag{3.37}$$

Equations (3.19) and (3.21) yield an implicit expression for T_b in terms of φ,

$$\delta = J(T_b) \equiv \frac{\varepsilon B q \alpha^{-1} (T_b - T_o)^{-1} \log(T_b/T_o) - \mu_o \delta F(1-\varphi)}{F + (1-F)\varphi}. \tag{3.38}$$

The dimensional version of this expression is

$$\tilde{\alpha}\mu \tilde{Y}_o^{-1}(L\tilde{f}_- + (\tilde{f}_+ - \tilde{f}_-)\phi) = g\tilde{\rho}_{go}^2 \tilde{Q}(\tilde{T}_b - \tilde{T}_o)^{-1} \log(\tilde{T}_b/\tilde{T}_o) - \mu_g \tilde{\alpha}\tilde{f}_-(L-\phi). \tag{3.39}$$

The unknowns V_+, V_-, U, and η_b are then given by (3.17)–(3.20) as

$$V_+ = \delta (T_b - T_o)^{-1} q^{-1} \sqrt{C^2 + 4\alpha}, \tag{3.40}$$

$$V_- = V_+(1+\mu_o), \qquad U = C + V_-, \qquad \eta_b = V_+/(\delta U). \tag{3.41–3.43}$$

Notice that the restriction $\eta_b < 1$ implies we must have

$$\left[\left(\frac{qT_b}{T_b - T_o}\right)^2 \mathrm{e}^{E(1-1/T_b)} - \alpha\right] q > (1 - \delta(1+\mu_o))(T_b - T_o)$$
$$\times \left[\left(\frac{qT_b}{T_b - T_o}\right)^2 \mathrm{e}^{E(1-1/T_b)} + \alpha\right]. \tag{3.44}$$

For each set of parameters, we must use (3.38) to determine the potential solution for T_b and then test it to see if that solution exists.

As one might expect by the similarity in exponential decay in temperature, the reaction-trailing and reaction-leading structures yield similar curves depicting the dependence of T_b and other quantities on α (see Figure 7). The structure and temperature profiles are reversed, but the heat-transfer processes occur at the same rate, so T_b and U depend on α in a similar manner.

4. Conclusions

Upward buoyant FC is both similar to and different from forced forward FC. It is similar in that, as in forced forward FC, a localized high-temperature domain (HTD), in which the tempera-

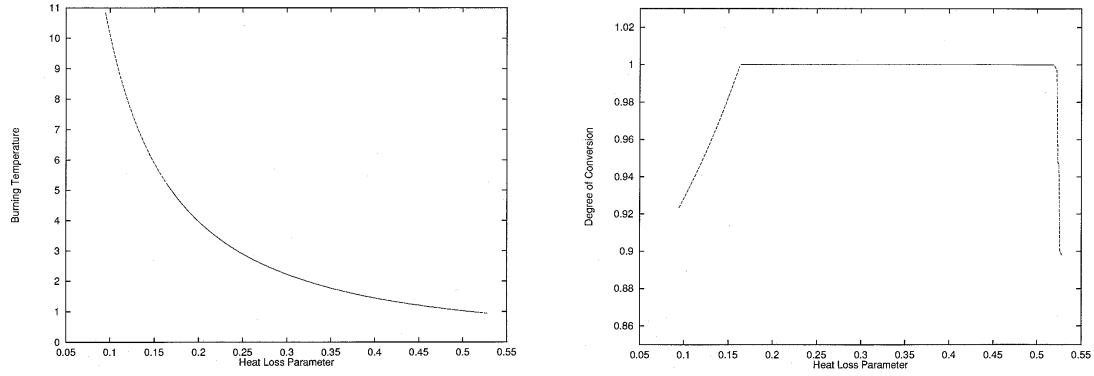

Figure 7. (a) Burning Temperature at the middle of the sample as a function of the heat-loss parameter for reaction-trailing structure solutions. Stoichiometric (solid) and Kinetically-Controlled (dashed) solutions are indicated. (b) The Degree of Fuel Conversion associated with the solution in (a). Here, $T_o = 0{\cdot}2, \delta = 1{\cdot}15, E = 5, \varepsilon B = 0{\cdot}4, F = 1{\cdot}0, \phi = 0{\cdot}5$, and $\mu_o = 1{\cdot}0$.

ture is essentially constant, propagates along the sample. The length of the HTD grows slowly with time. The reaction can occur at the leading or trailing edge of the HTD, depending on the oxidizer mass fraction relative to stoichiometry. For $\delta(1 + \mu_o) > (<)1$, the reaction occurs at the leading (trailing) edge of the HTD. The resulting structure is referred to as a reaction leading (trailing). Ahead of and behind the HTD, the temperature is essentially constant at the cool temperature T_o, and there are thin layers connecting the HTD to the cool regions. They are the combustion layer and the heat-transfer layer. In the reaction-leading (trailing) structure, the combustion (heat-transfer) layer precedes the heat-transfer (combustion) layer. Super-adiabatic temperatures are attained (*cf.* (2.22)) as the incoming gas absorbs heat from the burned solid as it passes through the product region and transports it to the fresh solid fuel. The combustion waves are stoichiometric or kinetically controlled, depending on the relative rates of oxidizer supply and reaction kinetics. Equations (2.39) and (2.65) give conditions for the appearance of stoichiometric and kinetically controlled solutions. The conditions show that stoichiometric (kinetically controlled) combustion occurs when the oxidizer supply limits (does not limit) the reaction. That is, when the burned portion of the sample is sufficiently small (large), so that incoming flux is sufficiently small (large) that the reaction must (not) wait for additional gas in order to proceed along the sample.

One significant difference between forced forward FC and upward buoyant FC is that for the former, the incoming gas flux is fixed by external sources, while for the latter it is determined by buoyancy induced by the combustion process itself. Hot gas rises and pulls fresh gas in through the bottom of the sample. The fresh gas supplies oxidizer to the reaction which releases more heat and causes more gas to rise. Buoyancy-induced flux depends on the gravitational acceleration, the ambient pressure, the permeability of the porous matrix and on the total heating of the gas in the sample. Thus, the amount of incoming gas is determined by the size of the HTD which,in turn, is determined by the incoming gas flux. This buoyancy-induced feedback also causes the propagation velocity to vary with time (*cf.* (2.21)) as the HTD grows and more gas is available to feed the reaction, so that propagation will vary much

more rapidly in upward buoyant combustion than in the forced case. We also expect that for non-adiabatic conditions, the feedback can cause changes in stability and extinction limits compared to those for forced forward FC at the same incoming flux.

Another difference between forced forward FC and upward buoyant FC is that in the latter case the induced pressure gradient driving convection is small and limited by the hydrostatic pressure drop $(\rho g L)$ across the sample $(B = 0(1)$, *cf.* discussion of (1.27)). This means that combustion can only be realized in practice, if the permeability of the sample is high, since otherwise it would require an extremely long sample. In contrast, for forced flow the driving mechanism for convection is externally controlled, so that combustion can be realized, in principle, for any permeability, if the pressure drop is large enough to overcome the resistance of the sample.

In this paper, we determined the temperature profile including the burning temperature, propagation velocity, induced gas flux, oxidizer consumption, and degree of fuel conversion for the reaction-leading and trailing structures in both stoichiometric and kinetically controlled waves. Descriptions of the variation in these quantities as the wave propagates through the sample are obtained. As a general result, the intensity of combustion increases as the wave moves through the sample (*cf.* (2.21)). The propagation velocity, incoming gas flux and, in kinetically controlled cases, the burning temperature all increase as the heated portion of the sample increases (*cf.* (2.31)–(2.36)).

In addition, predictions of parameter regions which support each structure and mode are presented in terms of the parameters of the problem (*cf.* (2.39), (2.65), and (2.66)).

An analysis of the case in which the effect of heat losses to the external environment is important is also presented. One interesting result is that buoyant forces must be sufficiently large to support a wave when heat losses are significant. The heated region of the sample is relatively short for the large heat loss case, so that the amount of hot gas is small and buoyancy may not be sufficient to supply oxidizer to the reaction. Additional oxidizer can be supplied only by an increase of buoyancy forces through larger gravitational accelerations, *e.g.*, in a centrifuge, high initial gas density, or high permeability of the sample.

One effect of buoyancy in downward combustion [17] is that ignition may be difficult, because a significant portion of the sample must be heated to induce the incoming gas flux needed to support the combustion wave. This is true even for adiabatic conditions. In downward buoyant FC, the burning temperature depends on the amount of fuel converted which varies with the gas flux and thus with the size of the burned region of the sample. The burned region of the sample must be sufficiently large to insure a temperature which supports the reaction. The conditions for ignition thus require that a specific fraction of the sample be heated. In contrast, for upward combustion, ignition will occur as long as the temperature is sufficiently large to support a reaction. Even if only a small region of the sample is heated, so that the incoming gas flux is small, stoichiometric combustion will continue in which the burning temperature is independent of the length of the burned region (*cf.* (2.22), (2.57)–(2.58)). A high burning temperature is thus ensured as long as heat losses are not too large. The kinetically controlled mode of propagation only occurs for high gas fluxes (*cf.* (2.39), (2.65)). In this case, combustion is sufficiently intense that the temperature dependence on the length of the burned region is insufficient to affect ignition.

Heat losses can cause extinction in the kinetic mode of propagation, however, and weaken combustion in the stoichiometric case, until the wave becomes kinetically controlled (Figure 6). Small heat loss allows large temperatures which drive large incoming gas flux through the

sample. Thus, for small heat loss, the gas flux is large and kinetically controlled solutions are obtained (Figures 6a, 7). As heat losses increase, burning temperatures and gas flux decrease and the wave becomes stoichiometric, *i.e.*, propagation is determined by the oxidizer supply. Further increases in heat losses cause the wave to become kinetically controlled prior to extinction, which occurs when heat losses exceed a critical value.

Buoyant FC has been studied experimentally in [11, 12, 18, 19, 20]. These studies provide some insight into the controlling mechanisms of the process. Specifically, it was shown [11, 19] that diffusion does not play a significant role in supplying oxidant to the reaction. Rather, gravity-induced buoyant convection has been shown experimentally to be the dominant mechanism of supply. The effect of ambient pressure P_o on the process [19] was observed to be as predicted by theory. Specifically, the velocity of propagation was observed to vary as P_o^2, in agreement with our result. Note that the dependence of the velocity on P_o is the same in both the ignition and propagation stages, since it depends only on the nondimensionalization of the time dependent problem. The data in [11, 20] shows that even for such an extremely porous material as polyeurethane foam, with a void fraction which exceeds 90%, the effective Lewis number is large ($Le \sim 60$). All these experimentally facts are incorporated in our model. However, it appears that the lengths of the samples ($L \sim 20$ cm) employed in [11, 12, 18, 19] were insufficient for self-sustained buoyant FC waves to develop. Since the study of the properties of such waves is precisely the subject of this paper, it is difficult to make direct comparisons with experimental results, which can, at best, describe only the transient period of ignition. To make such direct comparisons, it would be necessary to perform experiments with longer samples and to measure independently the kinetic and thermophysical paramaters of the process. Our analysis does show that the primary kinetic parameter is the stoichiometric ratio μ of oxygen/fuel consumption. Together with the heat capacities of the gas and the solid, the value μ determines the structure of the wave. Specifically, it determines whether the structure is reaction-leading or reaction-trailing. It also determines the maximum temperature developed in the process. We show that this temperature may exceed the adiabatic temperature, calculated from thermodynamic arguments. The excess may be very large when μ attains a certain critical value. In this case the porous medium may be characterized as extremely dangerous from the point of view of fire safety.

We do not describe the transition to flaming. To do so would require more detailed models including multistep kinetics and phase transitions. We simply draw attention to the fact that the temperature can reach quite high levels, which *may* initiate the transition process. We note that the self-sustained quasisteady buoyant FC waves that we describe require porous samples whose length is sufficiently larger than the length l_c of the preheat layer, which can be estimated as the ratio of the thermal diffusivity to the velocity of propagation.

5. Acknowledgement

Supported in part by NASA Grant NAG3-1608, D.O.E. Grant DE-FG02-87ER25027, International Science Foundation and Russian Government Grant J19100 and NASA GSRP Fellowship NTG-50902.

Declaration of the symbols

B	Nondimensional buoyant flux
c	Heat capacity
$\tilde{c}_1$	Effective heat capacity of sample
C	Nondimensional difference of products of velocities and heat capacities
D	Diffusion coefficient
$\tilde{E}$	Activation energy
E	Nondimensional activation energy
$\tilde{f}$	Filtration coefficient
f	Nondimensional filtration coefficient
F	Ratio of filtration coefficients
g	Gravitational acceleration
H	Heaviside step function
K_o	Pre-exponential factor
ℓ	Nondimensional length of high-temperature domain
l_C	Length of combustion layer
l_h	Length of heat-transfer layer
l_{HTD}	Length of high-temperature domain
l_α	Length scale of cooling
L	Length of sample
Le	Lewis number
P	Nondimensional pressure
p	Ratio of ambient pressure and hydrostatic pressure drop
$\tilde{P}$	Effective gas pressure
q	Nondimensional heat release
$\tilde{Q}$	Heat release of reaction per unit mass of solid reactant
r	Ratio of gas to solid heat capacities per unit volume
R	Universal gas constant
$\tilde{R}$	R/(molecular weight of gas)
$\tilde{t}$	Temporal variable
t	Nondimensional temporal variable
$\tilde{T}$	Temperature
T	Nondimensional temperature
$\tilde{\mu}$	Combustion wave velocity
U	Nondimensional combustion wave velocity
$\tilde{v}_g$	Gas velocity
V	Nondimensional gas flux through reaction site
$\tilde{W}$	Reaction rate
W	Nondimensional reaction rate
$\tilde{x}$	Spatial variable
x	Nondimensional spatial variable
X	Spatial variable on scale of combustion layer
$\tilde{Y}$	Oxidizer mass fraction
Y	Oxidizer mass fraction scaled by ambient mass fraction
Z	Zeldovich number
$\tilde{\alpha}$	Heat-loss coefficient
α	Nondimensional heat-loss coefficient
δ	Ratio of gas to solid heat capacities
ε	Length of combustion layer on scale of sample
η	Degree of conversion
λ	Thermal conductivity
μ	Stoichiometric coefficient oxygen/solid
μ_g	Stoichiometric coefficient gas/solid
μ_o	Ratio of gas/oxygen stoichiometric coefficients
π	Porosity of the sample
ϕ	Position of reaction front
φ	Nondimensional position of reaction front
$\tilde{\rho}_g$	Effective gas density
$\tilde{\rho}_s$	Effective solid density
ρ	Nondimensional effective gas density
ζ	Time dependent spatial coordinate on which heat-transfer layer is stationary

Subscripts and superscripts

b	Evaluated at reaction front
cr	Critical value
g	Gas
s	Solid
$*$	Reference value
o	Initial or ambient value
$-, +$	Fresh fuel, product
so	Initial solid
go	Initial gas
ad	Adiabatic

References

1. A. P. Aldushin, Filtration Combustion. In: S. M. Frolov (ed.) Proceedings of the Zeldovich Memorial International Conference on Combustion Volume 1, Moscow (1993) 65–83.
2. A. P. Aldushin and B. S. Seplyarsky. Propagation of waves of exothermal reaction in porous medium during gas blow-through. *Soviet Physics - Doklady* 23 (1978) 483–485.
3. A. P. Aldushin and B. S. Seplyarsky, Inversion of the structure of a combustion wave in a porous medium during blow-through of gas. *Soviet Physics - Doklady* 24 (1979) 928–930.
4. T. J. Ohlemiller and D. A. Lucca, An experimental comparison of forward and reverse smolder propagation in permeable fuel beds. *Combust. Flame* 54 (1983) 131–147.
5. D. A. Schult, B. J. Matkowsky, V. A. Volpert and A. C. Fernandez-Pello, Propagation and Extinction of Forced Opposed Flow Smolder Waves. *Combustion and Flame* 101 (1995) 471–490.
6. D. A. Schult, B. J. Matkowsky, V. A. Volpert and A. C. Fernandez-Pello, Forced Forward Smolder Combustion. *Combustion and Flame* 104 (1996) 1–26.
7. J. L. Torero, M. Kitano and A. C. Fernandez-Pello, Forward smoldering of polyurethane foam. Presented at the Combustion Institute, Western States Section, Fall Meeting, Boulder Co., March 1991, Paper 91–27.
8. J. L. Torero, A. C. Fernandez-Pello and M. Kitano, Opposed forced flow smoldering of polyurethane foam. *Combust. Sci. and Technol.* 91 (1993) 95–117.
9. K. G. Shkadinsky, G. V. Shkadinskaya, B. J. Matkowsky and V. A. Volpert, Combustion Synthesis of a Porous Layer. *Combust. Sci and Technol.* 88 (1992) 247–270.
10. K. G. Shkadinsky, G. V. Shkadinskaya, B. J. Matkowsky and V. A. Volpert, Self-Compaction or Expansion in Combustion Synthesis of Porous Materials. *Combust. Sci. and Technol.* 88 (1992) 271–292.
11. J. L. Torero and A. C. Fernandez-Pello, Natural convection smolder of polyurethane foam, upward propagation. *Fire Safety Journal* 24 (1995) 35–52.
12. J. L. Torero and A. C. Fernandez-Pello and D. Urban, Experimental observations of the effects of gravity changes on smoldering. *AIAA Journal* 32 (1994) 991–996.
13. M. Fatehi and M. Kaviany, Adiabatic reverse combustion in a packed bed. *Combustion and Flame* 99 (1994) 1–17.
14. A. P. Aldushin, New Results in the Theory of Filtration Combustion. *Combustion and Flame* 94 (1993) 308–320.
15. E. W. Voice and R. Wild, Importance of heat transfer and combustion in sintering. *Iron and Coal Trades Review* 175 (1957) 841–850.
16. A. Egerton, K. Gugan and F. J. Weinberg, The mechanism of smoldering in cigarettes. *Combustion and Flame* 7 (1963) 63–78.
17. A. P. Aldushin, B. J. Matkowsky and D. A. Schult, Downward buoyant filtration combustion. *Combustion and Flame* 107 (1996) 151–175.
18. D. Stocker, S. Olson, J. L. Torero and A. C. Fernandez-Pello, Microgravity smoldering combustion on the USML-1 space shuttle mission. HTD- Vol. 269, Eds., Avedisian, C. T., and Arpaci, V. A. (1993) Book No. H00889.
19. S. Dosanjh, J. Peterson, A. C. Fernandez-Pello and P. Pagni, On smoldering combustion. *Acta Astronautica* 13 (1986) 659–696.
20. D. Stocker, S. Olson, D. Urban, J. L. Torero, D. Walther and A. C. Fernandez-Pello, Small scale smoldering combustion experiments in microgravity. *Twenty Sixth Intl. Symp. on Combustion*, Naples, Italy (1996) preprint.